Journal of Materials Chemistry

Cite this: *J. Mater. Chem.*, 2011, **21**, 3353

www.rsc.org/materials

**PAPER**

# Graphene modified $LiFePO_4$ cathode materials for high power lithium ion batteries

**Xufeng Zhou,[a] Feng Wang,[b] Yimei Zhu[b] and Zhaoping Liu*[a]**

***Received 30th September 2010, Accepted 3rd December 2010***
**DOI: 10.1039/c0jm03287e**

Graphene-modified $LiFePO_4$ composite has been developed as a Li-ion battery cathode material with excellent high-rate capability and cycling stability. The composite was prepared with $LiFePO_4$ nanoparticles and graphene oxide nanosheets by spray-drying and annealing processes. The $LiFePO_4$ primary nanoparticles embedded in micro-sized spherical secondary particles were wrapped homogeneously and loosely with a graphene 3D network. Such a special nanostructure facilitated electron migration throughout the secondary particles, while the presence of abundant voids between the $LiFePO_4$ nanoparticles and graphene sheets was beneficial for $Li^+$ diffusion. The composite cathode material could deliver a capacity of 70 mAh $g^{-1}$ at 60C discharge rate and showed a capacity decay rate of <15% when cycled under 10C charging and 20C discharging for 1000 times.



## Introduction

The demand for electrochemical-energy-storage systems with high capacity and high power grew at an unprecedented high speed over the last decade. Seemingly, one of the best solutions for these systems is the Li ion battery that exhibits great potential for outstanding performance.[1–3] Nevertheless, to meet such a demand, the rate capability of Li ion batteries must be improved, conceivably by exploiting novel electrode materials with better rate capability and cycling stability.

$LiFePO_4$ (LFP) cathode material has attracted much attention due to the low cost, low toxicity, and relatively large capacity.[4,5] However, the electrochemical performance of LFP deteriorates with increasing charge/discharge rates due to its low electronic conductivity and Li ion diffusion rate. Several strategies, such as carbon coating,[6–11] metal doping,[12–14] and particle size reduction,[15–20] have been developed to enhance the electrochemical performance. In particular, some recent work on the modification of LFP represents a significant progress made in the field. Wang *et al.* reported that a core–shell LFP/C nanocomposite prepared by an *in situ* polymerization restriction method could exhibit a capacity of 90 mA h $g^{-1}$ at charge/discharge rates of 60C.[9] Wu *et al.* suggested that a nanocomposite with highly dispersed LFP nanoparticles in a nanoporous carbon matrix could discharge at a rate up to 230C.[21] Kang and Ceder developed LFP nanoparticles coated with lithium phosphate, a fast ion-conducting surface phase; the material could be fully discharged in 10–20 s.[22] Though the current modification of LFP make it possible to achieve high power batteries, the cycling stability of the material at high rates (particularly >10C) remains a big challenge. Consequently, pursuing new modification methods is essential.

Recently, graphene[23,24] has shown great potential in Li ion battery applications. Improvement on cycling stability and rate capability were reported when some metal[25,26] or metal oxide[27–29] anode materials were modified by graphene. It was ascribed to the high conductivity and structural flexibility of graphene sheets. Such characteristics may also play an important role in enhancing the electrochemical performance of LFP cathode materials. Lately, Ding *et al.* prepared a LFP/graphene composite using a co-precipitation method.[30] However, there was no significant improvement in rate performance compared with conventional carbon coated LFP, because the LFP nanoparticles were only loosely loaded on graphene sheets, thereby resulting only in a limited enhancement in electron conductivity. Therefore, a better combination manner for LFP/graphene composite is needed to realize an optimum charge/discharge performance. In this paper, we describe a graphene modified LFP composite cathode material with excellent high rate capability and cycling stability, by creating a 3D network of graphene wrapping on LFP nanoparticles.

## Experimental

### Sample preparation

LFP nanoparticles were synthesized using a hydrothermal method reported in our previous paper.[31] Typically, 150 ml of 1 mol $L^{-1}$ $H_3PO_4$ aqueous solution was added to a beaker containing 600 ml of polyethylene glycol 400 whilst stirring it mechanically. Then, 450 ml of 1 mol $L^{-1}$ LiOH aqueous solution

[a]*Ningbo Institute of Material Technology & Engineering (NIMTE), Chinese Academy of Sciences, Ningbo, 315201, P. R. China. E-mail: liuzp@nimte.ac.cn; Fax: + 86 574 86685096*
[b]*Brookhaven National Laboratory, Upton, New York, 11973, USA*

was dropped into this mixture. When a milk white suspension formed *via* the neutralization reaction, 300 ml of 0.5 mol $L^{-1}$ $FeSO_4$ solution was poured into the beaker, generating a green colored suspension. The mixture was then transferred into a 2 L magnetic propelled autoclave, heated up to 180 °C at a rate of 3 °C $min^{-1}$ after sealing, and maintained at the same temperature under mechanical stirring for 9 h. After cooling down to room temperature, the off-white product was collected by centrifugation and washed three times in water. Finally, the resulting LFP nanoparticles were dispersed in DI water at a content of 50 wt%.

Graphene oxide (GO) was prepared following the procedure described in our previous report.[32] Typically, 6.0 g of $KNO_3$ and 5.0 g of natural graphite (300 mesh) were added to 230 ml of concentrated $H_2SO_4$ (98%) at room temperature. The mixture was stirred for 10 min before slow addition of 30 g of $KMnO_4$. Then, the mixture was heated to 35 °C and stirred for 6 h. Subsequently, 80 ml of water was added dropwise under vigorous stirring, causing a quick rise in temperature to ~90 °C. The slurry was stirred at this temperature for another 30 min. Afterwards, 200 ml of water and 6 ml of $H_2O_2$ solution (30 wt%) were added sequentially to dissolve insoluble manganese species. The resulting graphite oxide suspension was washed repeatedly in water until the solution pH reached a constant value of ~5.0. The complete delamination of graphite oxide into GO was achieved by ultrasonic treatment. The final suspension of GO was concentrated to a content of 1–2 wt%.

Aqueous suspensions of LFP and GO then were vigorously stirred together to form a slurry with LFP : GO = 10 : 1 (wt.). DI water was added to the mixture to adjust the solid content to 10 wt%. Thereafter, the slurry was stirred, and ultrasonically exposed for 5 min, and then spray dried at 200 °C to form a solid LFP/GO composite. The composites were heated to 600 °C at a rate of 5 °C $min^{-1}$ and annealed at that temperature for 5 h under Ar to form the active LFP/graphene (denoted by LFP/G) cathode materials.

For the preparation of conventional carbon-coated LFP (denoted by LFP/C), glucose monohydrate was used instead of GO (with a 5 : 1 weight ratio of LFP to glucose monohydrate) while keeping other conditions constant. Similarly, a mixture of GO and glucose monohydrate (LFP : GO : glucose monohydrate = 20 : 1 : 2 (wt.)) was employed to prepare LFP cathode materials with mixed carbon additives (denoted by LFP/(G + C)). In all three cases, the carbon contents in the final cathode materials were ~5 wt%.

### Structural characterizations

Scanning electron microscopy (SEM) and transmission electron microscopy (TEM) images were acquired with a Hitachi S-4800 field emission scanning electron microscope operated at 15 kV, and the Tecnai F20 transmission electron microscope at 200 kV, respectively. Electron energy-loss spectroscopy (EELS) and the corresponding high-resolution imaging, with and without energy filtering, were carried out using the JEM-3000F microscope equipped with a Gatan image filter (GIF) spectrometer. Raman spectra were recorded on a J-Y LabRam-IB spectrometer using 3 mW of 632.8 nm radiation from a He–Ne laser.

### Electrochemical measurements

For the preparation of the electrodes, the active materials (80 wt%), Super P (15 wt%) and poly(vinylidene fluoride) (5 wt%) were mixed in N-methyl-2-pyrrolidone and stirred for 10 h. The resultant slurry, pasted on Al foil, was dried at 80 °C under vacuum for 6 h. The loading density of the electrode is 3–4 mg $cm^{-2}$. The coin cells (2032) then were assembled in an argon-filled glove box using lithium metal as the anode, Celgard 2600 as the separator, and 1 M $LiPF_6$ (dissolved in ethylene carbonate and dimethyl carbonate with a 1 : 1 volume ratio) as the electrolyte. Cells were tested at room temperature using a LAND-CT2001A battery cycler (Wuhan, China) within the voltage range of 2.0–4.2 V (*vs.* $Li^+$/Li).

## Results and discussion

Fig. 1 illustrates the preparation process of the LFP/graphene composite (LFP/G). A spray drying technique was employed to prepare the LFP/graphene oxide composite, a precursor of LFP/G, from a mixed aqueous suspension of LFP nanoparticles and GO nanosheets. The reason that we did not use graphene nanosheets is that GO nanosheets are highly hydrophilic and thus miscible with the LFP nanoparticles. The as-prepared LFP/graphene oxide composite was then converted to LFP/G through annealing under argon atmosphere, during which GO was thermally reduced to graphene.

A typical SEM image shown in Fig. 2a shows that the LFP/G sample consists of secondary quasi-spherical microparticles with diameters of 2~5 μm. SEM observation at a higher magnification (Fig. 2b) reveals that each microsphere is actually a random aggregate of primary LFP nanoparticles that are covered by soft graphene sheets. The electron energy-loss spectroscopy (EELS) elemental map (Fig. 2c, d) further demonstrates that the LFP nanoparticles (in red) are wrapped loosely and imperfectly by a thin film of graphene (in green). TEM observation on the edge of individual microspheres (Fig. 2e) reveals that there are a considerable amount of voids between the nanoparticles and the sheets. The existence of voids indicates that the nanoparticles are wrapped, rather than coated, by the graphene sheets. The high resolution TEM image (inset of Fig. 2e) shows that the carbon film has a thickness of about 2 nm and consists of 3–5 layers of graphene. The interlayer distance is measured to be approximately 0.4 nm, slightly larger than the graphite lattice spacing of $d_{0002}$ (0.34 nm). Since the GO sheets we used were

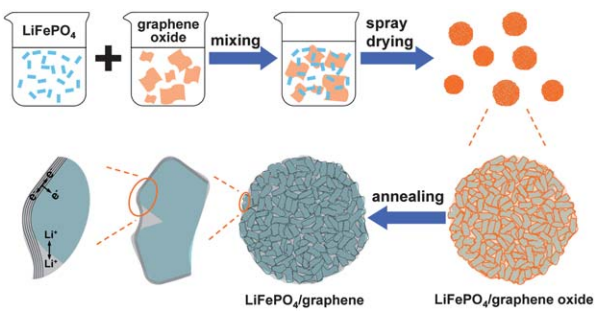


**Fig. 1** Illustration of the preparation process and the microscale structure of LFP/graphene composite.

 

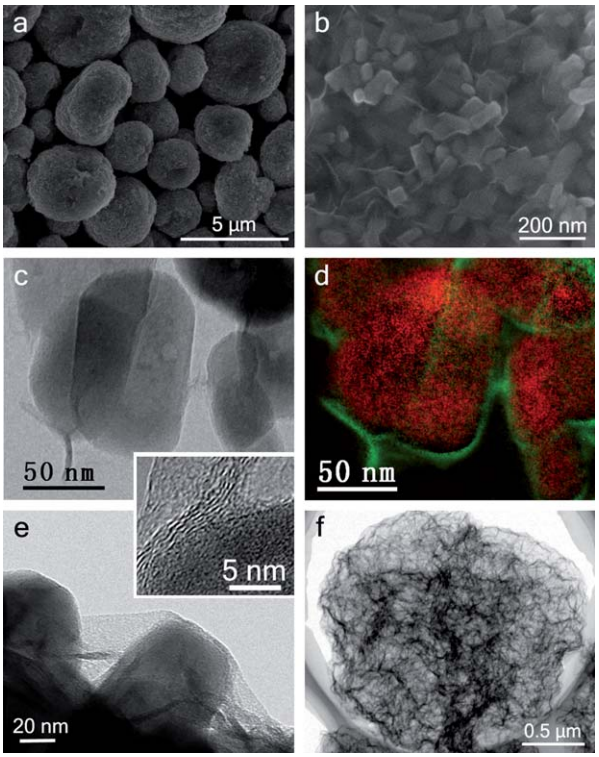


**Fig. 2** (a,b) SEM images showing an overview of the LFP/G particles. (c) TEM image, and (d) corresponding elemental map using EELS of the same area showing graphene-sheets wrapping on LFP nanoparticles, where red represents the LFP nanoparticles, obtained from the P L-edge, and the green represents graphene sheets, obtained from C K-edge. (e) TEM image on the edge of individual microspheres. The inset is a high-resolution TEM image illustrating the 3–5 monolayer thickness of the graphene-sheets on the surface of an individual LFP nanoparticle. (f) TEM image showing a 3D graphene network obtained by removing LFP nanoparticles with an HCl solution.

mostly single-layered, we believe that the multilayer structure of the wrapping graphene was formed by stacking and/or folding of the flexible GO sheets during the spray drying process. To further clarify the distribution of graphene in three-dimension, we treated the LFP/G composite with an HCl aqueous solution to remove the LFP nanoparticles. As expected, the foam-like residuals consist of a quasi-spherical 3D graphene network, as clearly illustrated by the TEM image (Fig. 2f). Apparently, the 3D network inherits the shape of the pristine LFP/G composite and suggests a homogenous distribution of graphene sheets in the secondary particles.

For comparison, a LFP/carbon composite (LFP/C) and a graphene modified $LiFePO_4$/carbon composite (LFP/(G + C)) were prepared by the same procedure. For the preparation of LFP/C, glucose, the common carbon source for LFP coating, was employed; while for the LFP/(G + C), a mixture of GO and glucose were used. Both composites show a similar morphology and size distribution (Fig. 3a, b) to LFP/G. However, the characteristic sheet-like carbon observed in LFP/G is not evident in the LFP/C (Fig. 3c, e). Apparently, the pyrolysis of glucose cannot result in large, continuous carbon layers. In contrast, LFP/(G + C) shows little differences, from LFP/G, in the structural characteristics (Fig. 3d, f).

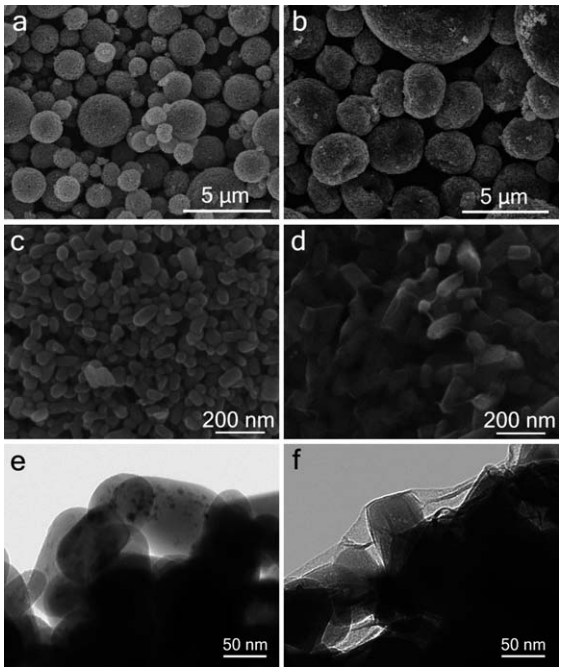


**Fig. 3** (a) SEM image of LFP/C secondary particles. (b) SEM image of LFP/(G + C) secondary particles. (c) SEM image with a high magnification showing the surface of an individual LFP/C secondary particle. (d) SEM image at high magnification showing the surface of an individual LFP/(G + C) secondary particle. (e) TEM image illustrating a local area of one LFP nanoparticle in an LFP/C secondary particle. (f) TEM image showing a local area of one LFP nanoparticle in an LFP/(G + C) secondary particle.

High resolution TEM images reflecting fine structure of graphene or carbon coating layers are shown in Fig. 4. It is found that the graphene sheets have a relatively regular stacking state in LFP/G (Fig. 4a). In some local areas, the stacking of graphene layers in LFP/(G + C) is, to some degree, less ordered than that in LFP/G, despite the layer-by-layer feature is obviously discernable (Fig. 4b). However, only amorphous coating layers, and no layered structure that is characteristic of graphitized carbon can be observed in LFP/C (Fig. 4c).

Raman spectra (Fig. 5) were presented to further identify the degree of graphitization of the carbon in the samples. LFP/G and LFP/(G + C) have almost identical Raman spectra, and the full width at half-maximum of both the D band and G band for the LFP/G and LFP/(G + C) is apparently smaller than that of LFP/C, suggesting that the thermally reduced graphene has a higher

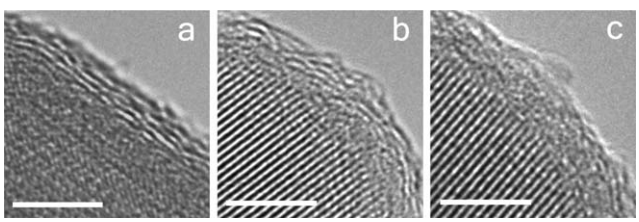


**Fig. 4** High resolution TEM images focuing on the surface of individual LFP nanoparticles in (a) LFP/G, (b) LFP/(G + C) and (c) LFP/C. All scale bars correspongd to 5 nm.

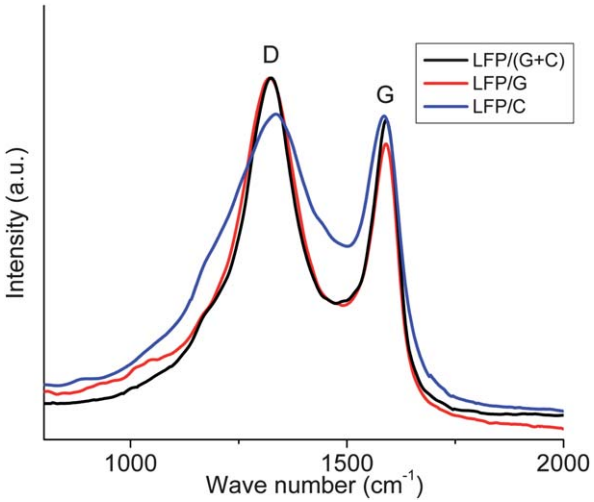


**Fig. 5** Raman spectra of LFP/C, LFP/(G + C), and LFP/G.

degree of graphitization than the glucose-derived carbon. The XPS spectra (Fig. 6) of three samples were also compared. It is apparent that the content of sp3 hybridized carbon atoms and C═O species is much higher for LFP/C than those for LFP/G and LFP/(G + C), which further verifies the results from Raman spectra that graphene sheets from GO is graphitized in a higher degree than carbon coating layers from glucose. It is interesting to note that the ratio of sp2 hybridized carbon atoms to sp3 hybridized ones for LFP/(G + C) is even a bit higher than that for LFP/G. It suggests that the mixing of GO and glucose still forms highly graphitized carbon species which are comparable to the case of pure graphene, though the graphene sheets stack in a less ordered way than those in LFP/G.

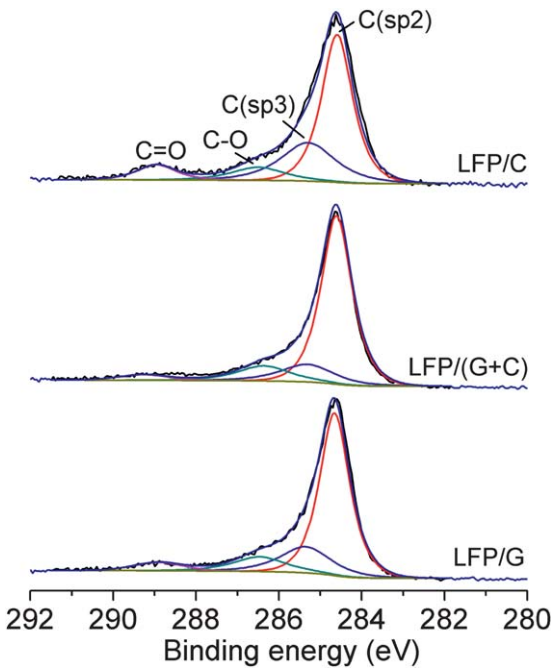


**Fig. 6** XPS spectra of LFP/G, LFP/(G + C), and LFP/C.

The as-prepared LFP/G, LFP/C and LFP/(G + C) cathode materials were assembled into coin cells to evaluate their electrochemical performances. As illustrated in Fig. 7, the three materials have the similar level in terms of discharge capacity at charge/discharge rates up to 5C, whereas the LFP/G and LFP/(G + C) possess a distinctly higher capacity than LFP/C at higher rates, suggesting the graphene modification can give rise to an excellent high rate performance. The LFP/G can deliver a capacity of $\sim$ 86 mA h $g^{-1}$ at the rate of 30C, reaching $\sim$60% of the initial capacity (148 mA h $g^{-1}$) at 0.1C. Unexpectedly, LFP/(G + C) displays better rate performance than LFP/G; it reached a capacity of 70 mA h $g^{-1}$ ($\sim$ 47% of the initial capacity at 0.1C) at a discharge rate as high as 60C. In comparison with the excellent performance of LFP/G and LFP/(G + C), the discharge capacity of LFP/C at 30 C is 54 mA h $g^{-1}$ ($\sim$ 40% of the initial capacity at 0.1C). Moreover, the discharge voltage of LFP/C at 30C is only comparable to those of LFP/G at 50C and LFP/(G + C) at 60C.

The high-rate cycling performances of the three materials were also investigated (Fig. 8). At 10C charge rate and 20C discharge rate, the LFP/C can deliver a discharge capacity of 90 mA h $g^{-1}$; after 1000 cycles, the capacity retention is about 70% of the initial capacity. In contrast, both LFP/G and LFP/(G + C) show much better cycling stability at the high rates. The LFP/G has a capacity decay rate of 15% when charging at 10C and discharging at 20C for 1000 cycles. The LFP/(G + C) exhibits cycling performance even better than LFP/G. At the same charging-discharging conditions, the capacity decay rate of LFP/(G + C) is as small as $\sim$ 5% after 1000 cycles. To the best of our knowledge, such a high-rate cycling performance for LFP is superior to the best results reported in the literature.[9,21,22]

The graphene-modified LFP materials described in this paper have reached high rate capability and excellent cycling stability under fast charge/discharge conditions. The progress achieved here is ascribed to three main factors. Firstly, the nanosized LFP particles are a prerequisite as their shorter diffusion path reduces the time needed for $Li^+$ to migrate between the cathode and electrolyte. Secondly, graphene with higher degree of graphitization is more advantageous than the conventional carbon-layer coating in increasing the electron conductivity. Thirdly, and most importantly, the 3D network of graphene wrapping on the LFP nanoparticles plays a critical role in the outstanding performance. The 3D network of graphene offers a considerable benefit over conventional carbon coating in terms of enhancing the electron conductivity within the secondary particles. Continuous graphene layers wrapping homogeneously around the surface of LFP nanoparticles serve as a fast path for electron migration during charge/discharge processes, while the voids between the graphene layers and the bare surfaces of LFP nanoparticles facilitate the diffusion of $Li^+$ from LFP lattices into the electrolyte, and *vice versa*. It is important to note that LFP/(G + C) possesses better rate capability than LFP/G. It is expected that in LFP/(G + C), glucose-derived amorphous carbon species, which coexist with graphene, may interrupt the stacking of graphene sheets to a less ordered state compared to that of pure graphene sheets in LFP/G. Thus, the in-plane anisotropy of electronic migration within graphene layers is, to some extent, minimized and the $Li^+$ diffusion is enhanced by the defects in the graphene sheets.

 

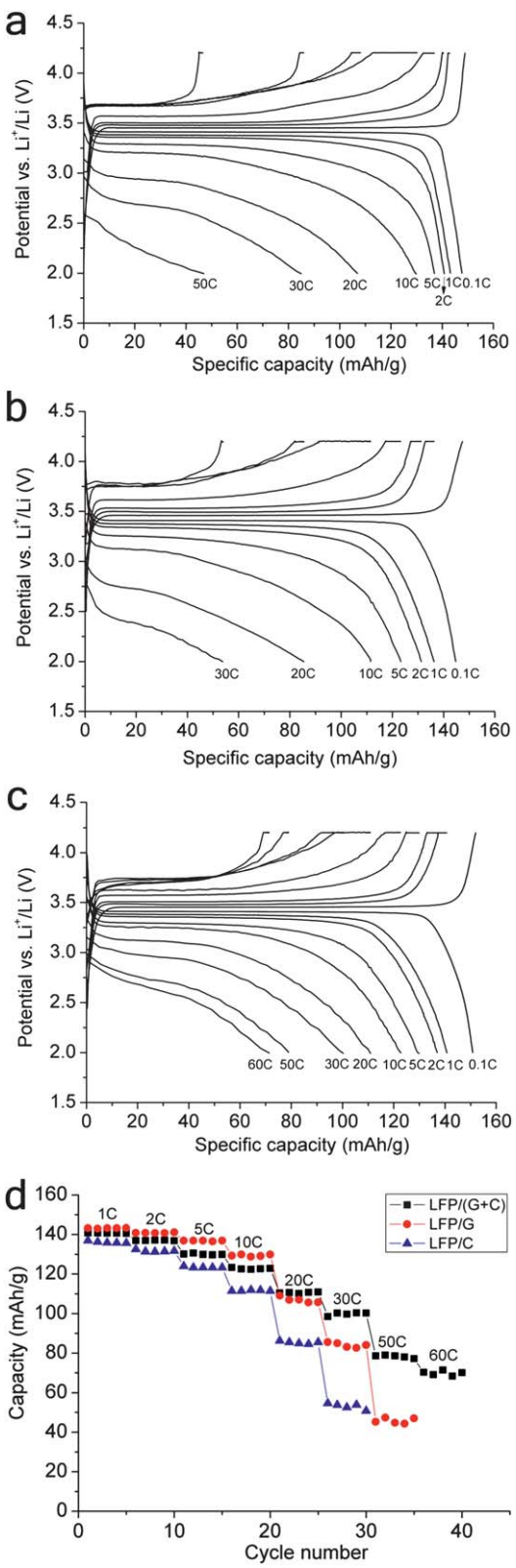


**Fig. 7** Rate discharge curves of (a) LFP/G, (b) LFP/C, and (c) LFP/(G + C). (d) Comparison of rate capability of LFP/G, LFP/C, and LFP/(G + C). Note that for LFP/G and LFP/C, the charging rate was the same to the discharging one when ≤10 C, and kept at 10C when the discharging one was >10C. For LFP/(G + C), the charging rate was the same to the discharging one when ≤20 C, and kept at 20C when discharging one was >20C.

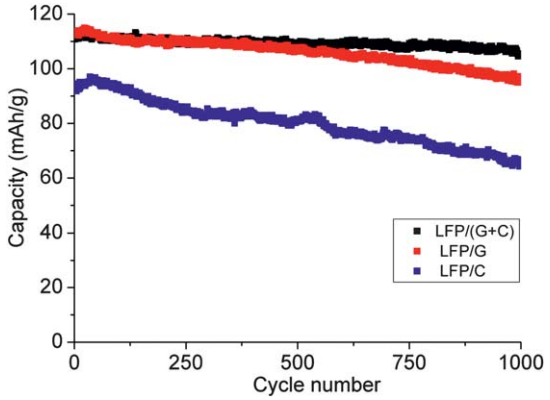


**Fig. 8** Comparative cycling performances of LFP/G, LFP/C, and LFP/(G + C) operated under 10 C charging and 20C discharging.

## Conclusions

We have succeeded in preparing graphene-modified LFP cathode materials with excellent high-rate capability and cycling stability. Using the spray-drying technique, we assembled LFP nanoparticles and graphene nanosheets in a manner that graphene sheets loosely wrapped on LFP nanoparticle. Furthermore, graphene sheets inside the microspheres are integrated into a continuous 3D conductive network that supports the maximum fulfilment of graphene's functionality since electrons are easily transferred between the surface of LFP nanocrystals and graphene, and move unobstructed over the nanoparticles to attain a high rate capability. In addition, the relatively simple availability of GO nanosheets and the high efficiency of spray drying facilitate scaling up this new cathode material for practical utilization. Consequently, our LFP/graphene composite cathode materials with their controlled microstructure and excellent rate performance and cycling stability offer great potential for applications in high-power electrical sources, such as electric vehicles. Moreover, the preparation strategy we developed is easily transferable to other cathode or anode materials with low conductivity to produce series of high-performance electrode materials, possibly shedding light on a new type of graphene-based Li-ion battery.

## Acknowledgements

We are grateful for financial support from the Chinese Academy of Sciences (Program of Knowledge Innovation, Grant No. KGCX2-YW-231-4 and KGCX2-YW-365; Program for Science and Technology Innovative Research Team of Ningbo Municipality, Grant No. 2009B21005), Zhejiang Provincial Natural Science Foundation of China (Grant No. R4100194 and Y4100499), and the Natural Science Foundation of Ningbo (Grant No. 2009A610046 and 2009A610029). Work at Brookhaven was supported by US DOE/BES under contract No. DE-AC02-98CH10886.

## References

1 J. M. Tarascon and M. Armand, *Nature*, 2001, **414**, 359.
2 M. Armand and J. M. Tarascon, *Nature*, 2008, **451**, 652.

3 P. G. Bruce, B. Scrosati and J. M. Tarascon, *Angew. Chem., Int. Ed.*, 2008, **47**, 2930.
4 A. K. Padhi, K. S. Nanjundaswamy and J. B. Goodenough, *J. Electrochem. Soc.*, 1997, **144**, 1188.
5 A. Yamada, S. C. Chung and K. Hinokuma, *J. Electrochem. Soc.*, 2001, **148**, A224.
6 Z. H. Chen and J. R. Dahn, *J. Electrochem. Soc.*, 2002, **149**, A1184.
7 R. Dominko, M. Bele, M. Gaberscek, M. Remskar, D. Hanzel, S. Pejovnik and J. Jamnik, *J. Electrochem. Soc.*, 2005, **152**, A607.
8 R. Dominko, M. Bele, J. M. Goupil, M. Gaberscek, D. Hanzel, I. Arcon and J. Jamnik, *Chem. Mater.*, 2007, **19**, 2960.
9 Y. G. Wang, Y. R. Wang, E. J. Hosono, K. X. Wang and H. S. Zhou, *Angew. Chem., Int. Ed.*, 2008, **47**, 7461.
10 M. M. Doeff, J. D. Wilcox, R. Kostecki and G. Lau, *J. Power Sources*, 2006, **163**, 180.
11 M. M. Doeff, J. D. Wilcox, R. Yu, A. Aumentado, M. Marcinek and R. Kostecki, *J. Solid State Electrochem.*, 2008, **12**, 995.
12 S. Y. Chung, J. T. Bloking and Y. M. Chiang, *Nat. Mater.*, 2002, **1**, 123.
13 P. S. Herle, B. Ellis, N. Coombs and L. F. Nazar, *Nat. Mater.*, 2004, **3**, 147.
14 N. Meethong, Y. H. Kao, S. A. Speakman and Y. M. Chiang, *Adv. Funct. Mater.*, 2009, **19**, 1060.
15 K. F. Hsu, S. Y. Tsay and B. J. Hwang, *J. Mater. Chem.*, 2004, **14**, 2690.
16 D. H. Kim and J. Kim, *Electrochem. Solid-State Lett.*, 2006, **9**, A439.
17 L. Laffont, C. Delacourt, P. Gibot, M. Y. Wu, P. Kooyman, C. Masquelier and J. M. Tarascon, *Chem. Mater.*, 2006, **18**, 5520.
18 B. L. Ellis, W. R. M. Makahnouk, Y. Makimura, K. Toghill and L. F. Nazar, *Nat. Mater.*, 2007, **6**, 749.
19 C. Delmas, M. Maccario, L. Croguennec, F. Le Cras and F. Weill, *Nat. Mater.*, 2008, **7**, 665.
20 P. Gibot, M. Casas-Cabanas, L. Laffont, S. Levasseur, P. Carlach, S. Hamelet, J. M. Tarascon and C. Masquelier, *Nat. Mater.*, 2008, **7**, 741.
21 X. L. Wu, L. Y. Jiang, F. F. Cao, Y. G. Guo and L. J. Wan, *Adv. Mater.*, 2009, **21**, 2710.
22 B. Kang and G. Ceder, *Nature*, 2009, **458**, 190.
23 K. S. Novoselov, A. K. Geim, S. V. Morozov, D. Jiang, Y. Zhang, S. V. Dubonos, I. V. Grigorieva and A. A. Firsov, *Science*, 2004, **306**, 666.
24 A. K. Geim and K. S. Novoselov, *Nat. Mater.*, 2007, **6**, 183.
25 G. X. Wang, B. Wang, X. L. Wang, J. Park, S. X. Dou, H. Ahn and K. Kim, *J. Mater. Chem.*, 2009, **19**, 8378.
26 J. K. Lee, K. B. Smith, C. M. Hayner and H. H. Kung, *Chem. Commun.*, 2010, **46**, 2025.
27 S. M. Paek, E. Yoo and I. Honma, *Nano Lett.*, 2009, **9**, 72.
28 D. H. Wang, D. W. Choi, J. Li, Z. G. Yang, Z. M. Nie, R. Kou, D. H. Hu, C. M. Wang, L. V. Saraf, J. G. Zhang, I. A. Aksay and J. Liu, *ACS Nano*, 2009, **3**, 907.
29 Z. S. Wu, W. C. Ren, L. Wen, L. B. Gao, J. P. Zhao, Z. P. Chen, G. M. Zhou, F. Li and H. M. Cheng, *ACS Nano*, 2010, **4**, 3187.
30 Y. Ding, Y. Jiang, F. Xu, J. Yin, H. Ren, Q. Zhuo, Z. Long and P. Zhang, *Electrochem. Commun.*, 2010, **12**, 10.
31 S. L. Yang, X. F. Zhou, J. G. Zhang and Z. P. Liu, *J. Mater. Chem.*, 2010, **20**, 8069.
32 X. F. Zhou and Z. P. Liu, *Chem. Commun.*, 2010, **46**, 2611.


 